DOI: 10.1002/ejic.200900940

1-D-Tin(II) Phenylchalcogenolato Complexes $^1_\infty[Sn(EPh)_2]$ (E = S, Se, Te) – Synthesis, Structures, Quantum Chemical Studies and Thermal Behaviour

Andreas Eichhöfer,*[a] Ji-Jun Jiang,[a,b] Heino Sommer,[c] Florian Weigend,[a] Olaf Fuhr,[a] Dieter Fenske,[a,c] Cheng-Yong Su,[b] and Gernot Buth[d]

Keywords: Tin / Chalcogens / Complexes / X-ray diffraction / TGA / Density functional calculations

A series of three 1-D-tin(II) phenylchalcogenolato complexes $^1_\infty[Sn(EPh)_2]$ (E = S, Se, Te) were synthesized in yields > 80 % by reaction of $SnCl_2$ with two equivalents of $PhESiMe_3$ in organic solvents. In the crystal the molecules form two different types of one-dimensional chains. In $^1_\infty[Sn(SPh)_2]$ the tin atoms are distorted trigonal pyramidal coordinated by sulfur atoms (two bonds within a monomer and one longer bond between neighbored monomers), while in $^1_\infty[Sn(EPh)_2]$ (E = Se, Te) the tin atoms show contacts to two neighbored monomers leading to a fourfold coordination of the tin atoms by either selenium or tellurium atoms. The bond situation is discussed on the basis of density functional calculations. Thermal treatment mostly leads to the formation of the corresponding phase pure tin(II) chalcogenides however sublimation plays an increasing role ongoing from the tellurolato to the thiolato complex especially for the use of vacuum conditions. The investigation of the volatile cleavage products reveals the occurence of more complex reactions in the gas phase than the formal stoichiometric cleavage of EPh_2 (E = S, Se, Te) with formation of SnE.

Introduction

Metal chalcogenolato complexes have attracted interest due to their rich structural chemistry,[1–3] their potential use as precursors for M/Se materials[4,5] and their relevance as models for active sites of chalcogen containing metalloproteins.[6,7]

Tin(IV)chalcogenolato complexes like $Sn(SPh)_4$,[8] $Sn(SePh)_4$[9,10] and $Sn(Se\text{-}2\text{-}NC_5H_4)_4$[11] as well as related tin(II) compounds like $[Sn\{ESi(SiMe_3)_3\}_2]_2$ (E = S, Se, Te)[12] and $[Sn(2\text{-}SeNC_5H_4)_2]_2$[11] have been studied in view of their use as precursor compounds for MOCVD of SnE and SnE_2 (E = S, Se) while the corresponding tin(II) compounds also attracted interest due to the synthesis of "carbene analogues" and the realisation of low coordination modes. Synthetic procedures for compounds with the general formula $Sn(ER)_2$ (E = S, Se, Te; R = organic group) are especially for thiolato complexes well established. With respect to the compounds under investigation $Sn(SPh)_2$[13–16] as well as $Sn(SePh)_2$[17] have been synthesized before while no report could be found for the tellurium analogue. However the structures of only a few compounds of this type are reported including monomeric $[Sn(S\text{-}2,4,6\text{-}tC_4H_9C_6H_2)_2]$,[18] dimeric $[Sn\{TeSi(SiMe_3)_3\}_2]_2$[12] and $[Sn(2\text{-}SeNC_5H_4)_2]_2$,[11] trimeric $[Sn(S\text{-}2,6\text{-}(iC_3H_7)_2C_6H_3)_2]_3$ as well as polymeric $^1_\infty[Sn(StC_4H_9)_2]$[19] and $^1_\infty[Sn(SnC_4H_9)_2]$.[20] The build up of the structures is mostly determined by the stereochemical effect of the "inert" electron pair and the interplay of the steric demand of the organic ligands vs. the tendency of tin(II) to realize higher coordination modes than two together with a minor influence of the kind of chalcogen element.

Reported here are the synthesis of three 1-D-Tin(II) phenylchalcogenolato complexes $^1_\infty[Sn(EPh)_2]$ (E = S, Se, Te) by reaction of $SnCl_2$ with two equivalents of $PhESiMe_3$ in organic solvents along with their structural characterization and an investigation of their thermal behaviour.

[a] Institut für Nanotechnologie, Forschungszentrum Karlsruhe, Postfach 3640, 76021 Karlsruhe, Germany
Fax: +49-7247-82-6368
E-mail: eichhoefer@int.fzk.de
[b] MOE Laboratory of Bioinorganic and Synthetic Chemistry and State Key Laboratory of Optoelectronic Materials and Technologies, School of Chemistry and Chemical Engineering, Sun Yat-Sen University,
Guangzhou 510275, P. R. China
[c] Institut für Anorganische Chemie der Universität, Engesserstrasse, Geb. 30.45, 76128 Karlsruhe, Germany
[d] Institut für Synchrotronstrahlung (ISS), Forschungszentrum Karlsruhe GmbH,
Postfach 3640, 76021 Karlsruhe, Germany
Supporting information for this article is available on the WWW under http://dx.doi.org/10.1002/ejic.200900940.

Results and Discussion

Synthesis and Structure

The tin(II) chalcogenolato complexes $^1_\infty[Sn(SPh)_2]$ (**1**), $^1_\infty[Sn(SePh)_2]$ (**2**) and $^1_\infty[Sn(TePh)_2]$ (**3**) were prepared by reaction of anhydrous $SnCl_2$ with two equivalents of $PhESiMe_3$ (E = S, Se, Te) in dme for **1** and **2** or thf for **3** in accordance to Scheme 1.

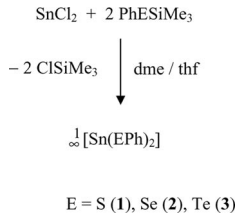

Scheme 1.

1 crystallizes in the orthorhombic space group *Pca*2$_1$ (Table 3). In the crystal structure the Sn(SPh)$_2$ units of **1** are μ_2-bridged in one dimension by one of the phenylthiolato ligands (S(2)) to form infinite chains along *a* (Figure 1) while the other SPh$^-$ group coordinates the tin atom as a terminal ligand. Two of the three Sn–S distances Sn(1)–S(1) [251.8(2) pm] and Sn(1)–S(2) [257.7(2) pm] are distinctly smaller than the contact between Sn(1) and S(2)′ with 273.1(2) pm. Although these shorter distances are slightly longer than the Sn–S bond [243.5(1) pm] found in monomeric [Sn(S-2,4,6-*t*C$_4$H$_9$C$_6$H$_2$)$_2$][18] one can therefore better describe the structure as consisting of monomeric Sn(SPh)$_2$ units which are linked by two additional weaker sulfur to tin donor-acceptor bonds to form the polymeric chains (see chapter Quantum Chemical Considerations). This leads in summary to a distorted trigonal pyramidal coordination around the tin atom [S–Sn(1)–S angles: S(1)–Sn(1)–S(2) 77.16(6), S(1)–Sn(1)–S(2)′ 92.68(6), S(2)–Sn(1)–S(2)′ 87.58(5)°]. The polymeric structure thus differs from those found for $^1_\infty$[Sn(S*t*C$_4$H$_9$)$_2$][19] and $^1_\infty$[Sn(S*n*C$_4$H$_9$)$_2$][20] where the tin atoms were found to be fourfold coordinated by the thiolato ligands. A similar trigonal pyramidal coordination was observed for two of the tin atoms in trimeric [Sn(S-2,6-(*i*C$_3$H$_7$)$_2$C$_6$H$_3$)$_2$]$_3$.[18]

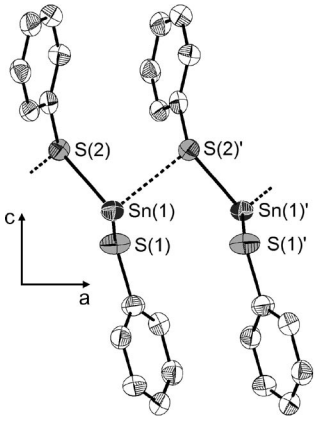

Figure 1. Section of the crystal structure of $^1_\infty$[Sn(SPh)$_2$] (**1**) viewed down *b* (50% ellipsoids, H atoms omitted for clarity). Symmetry transformation for generation of equivalent atoms: ′ *x* + 1/2, –*y* + 2, z. Selected bond length [pm]: Sn(1)–S(1) 251.8(2), Sn(1)–S(2) 257.7(2), Sn(1)–S(2)′ 273.1(2). Selected bond angles (°): S(1)–Sn(1)–S(2) 77.16(6), S(1)–Sn(1)–S(2)′ 92.68(6), S(2)–Sn(1)–S(2)′ 87.58(5), Sn(1)–S(2)′–Sn(1)′ 97.03(5).

2 crystallises in the monoclinic space group *P*2$_1$/*n* with two formula units in the asymmetric unit (Table 3). In contrast to **1** the Sn(SePh)$_2$ units of **2** are in the solid state μ_2-bridged in one dimension by both phenylselenolato ligands [Se(1), Se(2) and Se(3), Se(4)] to form infinite chains along *b* (Figure 2). Two of the Sn–Se distances [Sn(1)–Se(1): 266.87(8), Sn(1)–Se(2): 267.57(7), Sn(2)–Se(3): 268.32(7), Sn(2)–Se(4): 267.37(8) pm] are distinctly smaller than the "secondary" Sn–Se contacts [Sn(1)–Se(3) 291.45(7), Sn(2)–Se(2) 298.02(7), Sn(1)′–Se(4) 321.80(7), Sn(2)–Se(1)′ 310.73(7) pm]. The shorter Sn–Se distances are similar to those found in AsPh$_4$[Sn(SePh)$_3$] (264.9–267.0 pm)[21] and [Yb(C$_4$H$_8$O)$_6$][Sn(SePh)$_3$]$_2$ (262.9–268.5).[22] Therefore the crystal structure of **2** consists of Sn(SePh)$_2$ units [Se–Sn–Se angles: Se(1)–Sn(1)–Se(2) 88.15(3), Se(4)–Sn(2)–Se(3) 82.37(3)] which are linked by four additional weaker selenium to tin donor-acceptor bonds in order to form one dimensional chains. The polymeric structure is thus comparable to those found for $^1_\infty$[Sn(S*t*C$_4$H$_9$)$_2$][19] and $^1_\infty$[Sn(S*n*C$_4$H$_9$)$_2$].[20]

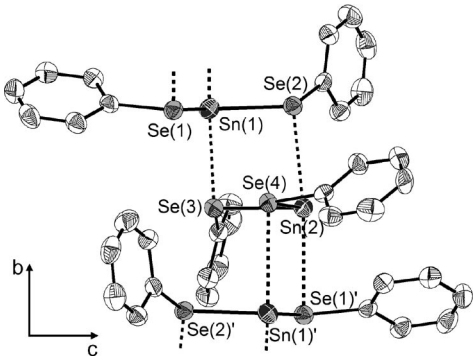

Figure 2. Section of the crystal structure of $^1_\infty$[Sn(SePh)$_2$] (**2**) viewed down *a* (50% ellipsoids, H atoms omitted for clarity). Symmetry transformation for generation of equivalent atoms: ′ –*x* + 1/2, *y* – 1/2, –*z* + 1/2. Selected bond length [pm]: Sn(1)–Se(1) 266.87(8), Sn(1)–Se(2) 267.57(7), Sn(2)–Se(3) 268.32(7), Sn(2)–Se(4) 267.37(8), Sn(1)···Se(3) 291.45(7), Sn(2)···Se(2) 298.02(7), Sn(1)′···Se(4) 321.8(1), Sn(2)···Se(1)′ 310.7(1). Selected bond angles (°): Se(1)–Sn(1)–Se(2) 88.15(3), Se(1)–Sn(1)–Se(3) 83.85(1), Se(2)–Sn(1)–Se(3) 86.37(1), Se(4)–Sn(2)–Se(3) 82.37(3), Se(4)–Sn(2)–Se(2) 83.00(1), Se(3)–Sn(2)–Se(2) 84.92(1), Sn(1)–Se(2)–Sn(2) 92.88(1), Sn(2)–Se(3)–Sn(1) 94.21(1).

3 crystallises also in the monoclinic space group *P*2$_1$/*n* with two formula units in the asymmetric unit (Table 3). Similar to **2** the Sn(TePh)$_2$ units of **3** are in the crystal μ_2-bridged in one dimension by both of the phenyltellurolato ligands [Te(1), Te(2) and Te(3), Te(4)] to form infinite chains along *b* (Figure 3). Different bond lengths and angles as well as different orientations of the phenyl rings lead to another crystal packing for the Sn(TePh)$_2$ units in **3** in comparison to **2** expressed by different lattice constants. However the bonding situation is similar to **2** with SnTePh$_2$ units [Sn(1)–Te(2) 287.2(1), Sn(1)–Te(1) 289.5(1), Sn(2)–Te(4) 287.9(1), Sn(2)–Te(3) 288.4(1) pm]; [Te(2)–Sn(1)–Te(1) 87.28(3), Te(4)–Sn(2)–Te(3) 91.31(3)] which are linked by weaker tellurium to tin donor acceptor bonds [Sn(1)–Te(4) 327.4(1), Sn(2)–Te(1) 312.8(1), Sn(1)–Te(3) 316.8(1), Sn(2)′–Te(2) 334.5(1) pm] to form the one dimensional chains. Two different Sn–Te bond length [280.0(1) and

295.6(1) pm] were also found in dimeric $[Sn\{TeSi(SiMe_3)_3\}_2]_2$[12] where the tin atoms adopt a distorted trigonal pyramidal coordination in the crystal.

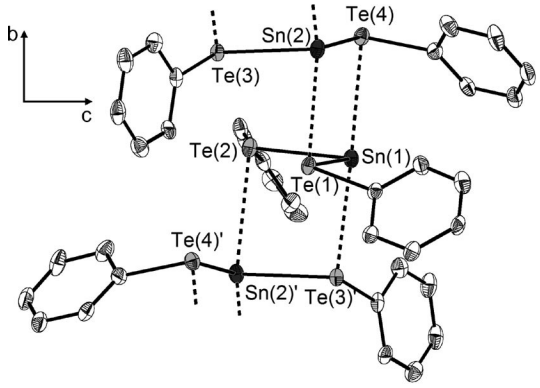

Figure 3. Section of the crystal structure of $^1_\infty[Sn(TePh)_2]$ (**3**) viewed down *a* (50% ellipsoids, H atoms omitted for clarity). Symmetry transformations for generation of equivalent atoms: $'$ $-x + 3/2$, $y - 1/2$, $-z + 1/2$. Selected bond length [pm]: Sn(1)–Te(2) 287.2(1), Sn(1)–Te(1) 289.5(1), Sn(2)–Te(4) 287.9(1), Sn(2)–Te(3) 288.4(1), Sn(1)···Te(4) 327.4(1), Sn(2)···Te(1) 312.8(1), Sn(1)···Te(3)′ 316.8(1), Sn(2)′···Te(2) 334.5(1). Selected bond angles (°): Te(2)–Sn(1)–Te(1) 87.28(3), Te(2)–Sn(1)–Te(3) 91.12(1), Te(1)–Sn(1)–Te(3) 78.06(1) Te(4)–Sn(2)–Te(3) 91.31(3), Te(4)–Sn(2)–Te(1) 89.20(2), Te(3)–Sn(2)–Te(1) 80.36(1), Sn(1)–Te(1)–Sn(2) 93.69(1), Sn(2)′–Te(3)–Sn(1) 92.28(1).

A comparison of the measured and calculated X-ray powder diffraction patterns for **1**, **2** and **3** reveal their crystalline purity with respect to the formation of other crystalline compounds (Figure S1). Slightly increasing differences in the position of the peaks with increasing detection angle arise from the temperature difference of the detection of the single crystal data and the powder patterns.

Optical Properties

Dried crystalline powders of **1**, **2** and **3** appear light-yellow, yellow and golden-yellow, respectively. The UV/Vis spectra in the solid state display a small shift in the absorption onset on going from **1** (440 nm) to **2** (470 nm) and a significant red shift for **3** (690 nm) (Figure 4). All spectra show only weakly pronounced features.

Upon going from **1** to **3** the solubility decreases significantly presumably due to the change in the structures as well as a stronger bonding of the large and soft base tellurolato ligands to the large and soft acid tin atoms compared to the thiolato and selenolato ligands. While **1** is well soluble in thf similar amounts of **2** need mixtures of more strongly coordinating solvents like CH_3CN and dmf. Although **3** shows some solubility in thf or CH_3CN it is only well soluble in dmso. However all solutions of **3** show upon standing decomposition indicated by the formation of black precipitates of SnTe as already observed for ether solutions of the related silylated compound $[Sn\{TeSi(SiMe_3)_3\}_2]_2$ by addition of Lewis bases like CH_3CN.[4]

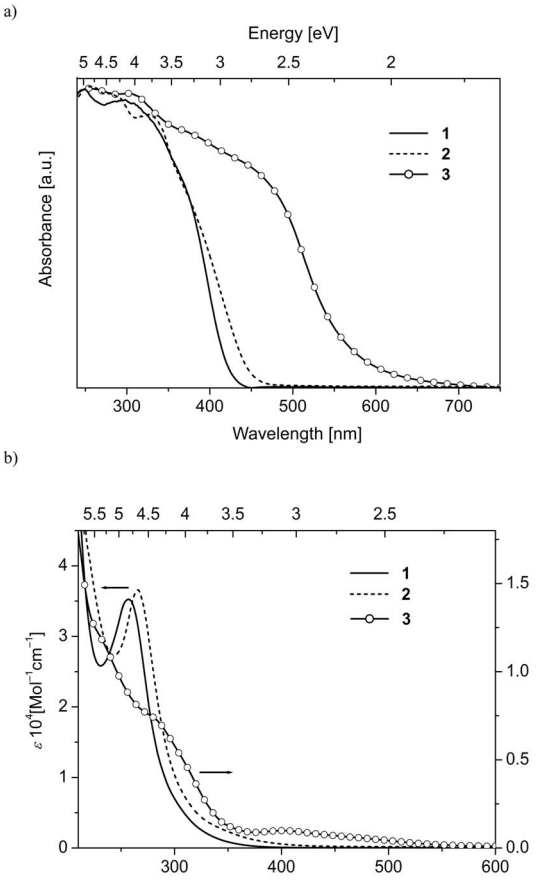

Figure 4. UV/Vis spectra of $^1_\infty[Sn(SPh)_2]$ (**1**), $^1_\infty[Sn(SePh)_2]$ (**2**) and $^1_\infty[Sn(TePh)_2]$ (**3**) a) in solid state (powder in mineral oil between quartz plates) and b) in thf.

UV/Vis spectra in thf display two nearly similar curves for **1** and **2** with maxima at 257 nm and 265 nm respectively most probably dominated by strong π-π* transitions of the chalcogenolato ligands (Figure 8). **3** although not completely soluble and slowly decomposing shows an onset of a weak and broad absorption already at 560 nm which might be assigned to ligand to metal charge transfer transitions followed by two shoulders at 280 nm and 232 nm. Calculation of the electronic triplet excitation spectrum of the mononuclear compounds $Sn(EPh)_2$ (E = S, Se, Te) with time-dependent density functional theory (for technical details see next section) reveals that the lowest excitations show a similar energetic shift from the sulfur to the tellurium species as observed in the measurements. However the strong red-shift which was especially observed in the solid state spectra of **3** compared to that of **2** is not reproduced in the calculations; calculated lowest excitations are at 1.8 eV(Te), 2.2 eV (Se) and 2.4 eV (S), see Figure S2 of the supplementary material. This discrepancy is not too surprising, as intermolecular interactions in the one-dimensional chains are not considered in the calculations. The lowest excitation mainly is a transition from the HOMO, located at the chalcogen atoms, to the LUMO, located

mainly at the Sn atom (Figure 5). Similar is true for the two excitations following in energy, so the lowest excitations are *p*-*p* ligand to metal charge transfer transitions.

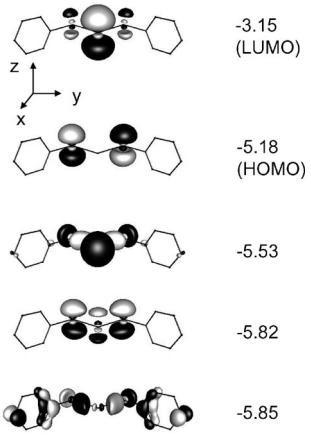

Figure 5. Molecular frontier orbitals of monomeric Sn(TeC$_6$H$_5$)$_2$. Contours are drawn at 0.05 a.u., orbital energies (right) are given in eV.

Quantum Chemical Considerations

The bond situation within a monomeric Sn(EPh)$_2$ (E = S, Se, Te) unit may be described by two-electron-two-centre E–Sn and E–C bonds. The remaining electrons form two lone pairs at each of the chalcogen atoms and one at the tin atom. For a better understanding and in order to rationalize the polymerization, density functional calculations (program system TURBOMOLE,[23] BP-86 functional,[24,25] def2-SV(P) bases[26] plus RI-J auxiliary bases,[27] effective core potentials for tin and tellurium[28,29]) were carried out. The frontier molecular orbitals for the monomer in C_{2v} symmetry with E = Te are shown in Figure 5; the shape is very similar for E = S, Se. The highest occupied molecular orbital (HOMO) is the antisymmetric combination of the *p*-orbitals of the tellurium atoms perpendicular to the molecular plane, p_z(Te). The HOMO-2 mainly consists of their symmetric combination plus small contributions from p_z(Sn). HOMO-1 and HOMO-3 are in the molecular plane; HOMO-1 consists of p_x(Sn) plus *s*(Sn) together with symmetry-matching combinations of p_x(Te) and p_y(Te); HOMO-3 involves p_y(Sn) and similar combinations from the tellurium atoms. The ratio of atomic contributions to the MOs and even their energetic sequence depend on spatial extension and energy difference of *s*- and *p*-orbitals of E (for E = Se HOMO-3 and HOMO-2 are interchanged, for E = S additionally HOMO-1 and HOMO). The lowest unoccupied orbital (LUMO) is the p_z(Sn) plus small contributions of p_z(Te). Agreement with the simple description given in the beginning of this section can be achieved by the consideration of localized molecular orbitals (LMOs); this is also helpful for understanding the mechanism of polymerization. LMOs are linear combinations of the occupied canonical MOs (CMOs), i.e. those resulting Hartree–Fock or DFT calculations (Figure 5); LMOs are obtained from CMOs by unitary transformation with the requirement that they have to be localized at as few as possible atoms (Pipek-Mezey localization[30]). In this way one loses the information of orbital energies, but gains objects that are suited for intuitive interpretation (bonds, lone pairs). We note that this transformation is not unique, i.e. different localization procedures will lead to slightly different LMOs. In Figure 6 (left hand side) we show the relevant LMOs located at tellurium and tin for the monomer: the Te–Sn and the Te–C bond (LMO1, LMO2), *s*-type lone pairs at tin and tellurium (LMO3, LMO4) and a *p*-type lone-pair at tellurium (LMO5). For the bonds also the contributions from the bond partners (from a Mulliken population analysis[31]) are shown. As expected, the Te–Sn-bond is significantly polarized towards the tellurium atom, the C–Te bond is slightly polarized towards the carbon atom.

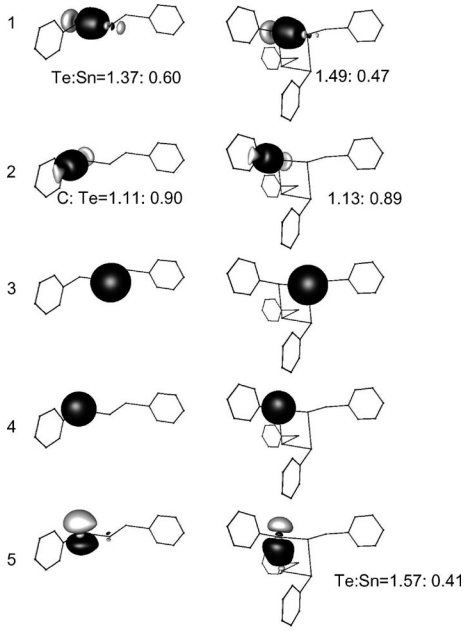

Figure 6. Selected localized molecular orbitals (Pipek-Mezey localization) of Sn(TeC$_6$H$_5$)$_2$ (left) and [Sn(TeC$_6$H$_5$)$_2$]$_2$ (right). Contours are drawn at 0.05 a.u. The numbers indicating the contributions from bond partners are calculated by a Mulliken population analysis.

Formation of polymers is studied for E = Te in detail, differences for E = S are given in the end. Polymerization is driven mainly by electron transfer from the p_z orbitals from the E atoms (electron donor, Lewis base) of one monomer to the empty p_z orbitals of the Sn atom (electron acceptor, Lewis acid) of a second monomer. This can be seen from the changes of some of the LMOs from the monomer to the dimer, right hand side of Figure 6. One observes significant electron transfer to the empty p_z orbital (LMO5) of the tin atom of the second monomer; the contribution of this atom to this LMO amounts to 0.41 electrons (from a Mulliken population analysis for this LMO). Further the polar character of the intramolecular Sn–Te-bond (LMO1) is enhanced; it is very similar to that of the intermolecular Sn–Te bond. In the same way electrons are trans-

ferred from p_z(Te) of the second unit to p_z(Sn) of the first unit. For each dimer the two remaining p_z(Te), which are not involved in this bond, are used to bind to the next dimer by the same mechanism. This on the other hand means that in each dimer the tin atoms act as acceptors for electrons from *two* further tellurium atoms (additional to that of the monomer).

For E = Se matters are very similar, but for E = S each tin atom is connected only to one further sulfur atom. This may have steric reasons, but also the lower energy of the *p*(S) orbitals compared to the *p*(Te) might be considered. This will lead to less pronounced electron transfer from sulfur to tin and thus to a preference for accepting electrons from only one additional sulfur atom. For clarity we finally note that the d-orbitals of Sn do not play a role in these considerations. This is confirmed by values for their occupation from natural population analyses (NPA),[32] which in all cases amount to less than 0.01 electrons.

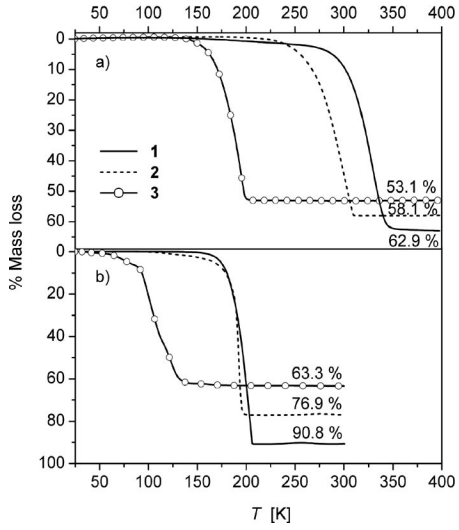

Figure 7. Thermogravimetric analysis of $^1_\infty$[Sn(SPh)$_2$] (**1**), $^1_\infty$[Sn(SePh)$_2$] (**2**) and $^1_\infty$[Sn(TePh)$_2$] (**3**) under a) He gas flow and b) in vacuo (see also Table 1).

Thermal Behaviour

Upon heating **1** starts to melt around 198 °C to give a brownish-yellow liquid and decomposes around 280 °C while **2** and **3** start to visibly decompose with formation of black powders already at 180 °C and 108 °C, respectively. In order to investigate the thermal properties of **1**–**3** in more detail we first performed thermogravimetric analysis under helium gas flow and under vacuum conditions. In addition thermolysis experiments were then carried out in Schlenk tubes to further investigate the cleavage products.

Thermogravimetric analyses under helium gas flow display clearly one step mass losses for **2** and **3** while **1** displays a minor gradual mass loss starting around 125 °C before the main decomposition step which occurs between 265 °C and 348 °C (Figure 7a, Table 1). The selenolato complex **2** decomposes between 200 °C and 310 °C while **3** is, as already indicated by its instability in solution, much more unstable than **1** and **2** and decomposes between 126 °C and 206 °C. The X-ray powder patterns of the residues reveal the formation of pure binary SnE (E = S, Se, Te) phases[33–35] (Figure S3) comparable with the pyrolysis products of the Sn^{VI} precursor molecules $(Ph_3Sn)_2E$ (E = S, Se, Te) which start to decompose around 330 °C.[36] Carbon and hydrogen contents were found to be less than 1%. While the experimental total mass loss for **3** is in good agreement with the calculated value for the formal cleavage of one equivalent of $TePh_2$ from $Sn(TePh)_2$ to yield SnTe according to Scheme 2, it differs for **1** and **2** (see Table 1).

Thermogravimetric analyses in vacuo in principle also display one step mass losses for **1**–**3** with two weak shoulders indicated for **3** (Figure 7b). Again, the tellurolate complex **3** decomposes much earlier, already between 50 °C and 145 °C, than **1** and **2**. The X-ray powder patterns of the residues of **2** and **3** indicate formation of pure orthorhombic SnSe and SnTe, respectively (C, H < 1%). Now for all compounds the experimental mass change is not in line with the calculated one according to Scheme 2 and Table 1.

Table 1. Experimental and theoretical mass loss (due to Scheme 2) for the thermal gravimetric analyses (Figure 7) of $^1_\infty$[Sn(SPh)$_2$] (**1**), $^1_\infty$[Sn(SePh)$_2$] (**2**) and $^1_\infty$[Sn(TePh)$_2$] (**3**).

Compound	Experimental mass loss [%]		Theoretical mass loss [%]
	He gas flow	vacuum	
1	62.4	90.8	55.3
2	58.1	76.9	54.1
3	53.1	63.3	53.4

$$Sn(EPh)_2 \xrightarrow{\Delta} SnE + EPh_2 \quad (E = S, Se, Te)$$

Scheme 2.

While for **3** the difference is about 10% for the thermal treatment of **2** the experimental mass loss of even more differs from its theoretical value compared to the TGA under helium atmosphere. For **1** the residue is only 9.2% in mass of the precursor complex and is characterised by powder XRD to be solely elemental tin suggesting not only sublimation but also a different thermal reaction than observed under atmospheric pressure.

In order to further investigate the cleavage products, thermolysis experiments were carried out in preparative scale (ca. 200 mg) under N_2 atmosphere (up to 350 °C) and in vacuo (up to 300 °C) in Schlenk tubes located inside a tube furnace (for details see experimental part and Table 2).

The cleavage products of the thermolysis of **1** under N_2 atmosphere could by careful condensation be almost completely separated in a yellow crystalline powder and a pale yellow liquid. However apart from the identification of the liquid main product SPh_2 by NMR[37,38] it was not possible to clearly identify the other compounds (see experimental section). In contrast, for the thermolysis of **1** under vacuum conditions only the formation of a light yellow solid precipitate on the walls of the glass tube outside the furnace is observed which is identified by powder XRD to consist

Table 2. Thermolysis data of $^1_\infty$[Sn(SPh)$_2$] (**1**), $^1_\infty$[Sn(SePh)$_2$] (**2**) and $^1_\infty$[Sn(TePh)$_2$] (**3**).

Compound	Final temperature [°C]	Residue[a]	Residual mass [%] (th.)[b]	Identified cleavage products[c]	Visible mp/decomp. [°C]
Thermolysis under N_2					
1	350	SnS	36.7 (44.7)	$S(Ph)_2$	198/280
2	350	SnSe	41.0 (45.9)	$Se(Ph)_2$	–/180
3	350	SnTe	46.0 (46.6)	$Te(Ph)_2$	–/108
Thermolysis under vacuum (2×10^{-6} mbar)					
1	300	Sn	8.2 (–)	$Sn(SPh)_2$, $Sn(SPh)_4$	198/–
2	300	SnSe	21.9 (45.9)		–/180
3	300	SnTe	36.0 (46.6)		–/110

[a] Identified by powder-XRD (C, H < 1%). [b] Calculated mass% of the residue due to the formal cleavage of one equivalent of $E(Ph)_2$ (E = S, Se, Te) (Scheme 2) with the exception of the vacuum thermolysis of $Sn(SPh)_2$ where 100% sublimation was assumed. [c] Identified by ^{1}H-, ^{13}C-NMR or powder XRD.

mainly of **1** (Figure 8). However the sublimation is accompanied by a partial decomposition reaction of **1** to give a 8.2% (TGA: 9.2%) mass percent residue of elemental tin and in the sublimate appropriate amounts of the oxidation product $Sn(SPh)_4$ as proven by the corresponding powder diffraction patterns[39,8] (26% decomposition product).

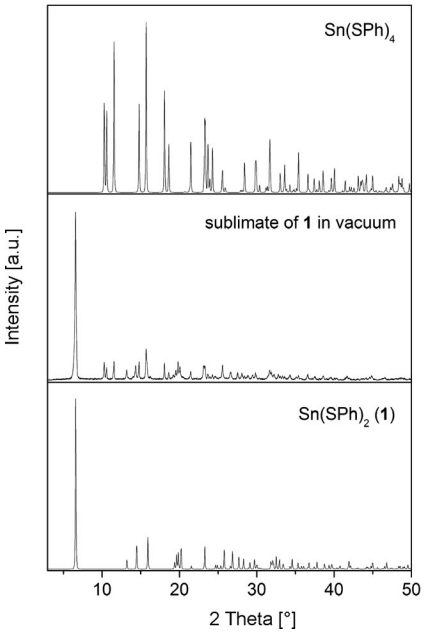

Figure 8. Powder XRD pattern of the cleavage products of the thermolysis of $^1_\infty$[Sn(SPh)$_2$] (**1**) under vacuum (2×10^{-6} mbar) compared with the calculated one of $Sn(SPh)_4$[8] and **1**.

The yellow cleavage product of the thermal treatment of **2** under nitrogen clearly display in the ^{1}H- and ^{13}C-NMR spectra peaks of the main product $SePh_2$[40,41] together with not yet identifiable additional peaks. Thermolysis of **2** under vacuum resulted also in the formation of a yellow liquid which condenses outside the furnace but in addition a black metallic mirror is formed on the walls of the glass tube inside the furnace. Due to the ^{1}H and ^{13}C NMR spectra the liquid cleavage products contain several not identifiable compounds while the black precipitate on the glass walls was characterized to be orthorhombic SnSe like the residue in the quartz boat. In line with the mass loss this suggests that **2** distinctly sublimes under the conditions of the experiment but decomposes at the hot walls of the tube before being able to leave the hot reaction zone.

Decomposition of **3** under N_2 atmosphere yields an orange oil as the cleavage product which was identified by ^{1}H- and ^{13}C-NMR to consist of $TePh_2$[42,43] with small amounts of unidentifiable side products. This is in agreement with the proposed reaction mechanism according to Scheme 2 and the results of the investigations of the thermolysis of $[Sn\{TeSi(SiMe_3)_3\}_2]_2$ which was reported to decompose cleanly at 250 °C to yield SnTe and $Te\{Si(SiMe_3)_3\}_2$.[12] In contrast ^{1}H and ^{13}C NMR spectra of the cleavage products from the thermolysis experiment of **3** under vacuum in a Schlenk tube (a red powder and a yellow liquid) show several signals for aromatic C and H atoms and do not clearly reveal the formation of $TePh_2$ which again indicates a more complex decomposition reaction then expected according to Scheme 2.

These findings are partially in agreement with observations on the thermal reactions of $[Sn\{ESi(SiMe_3)_3\}_2]_2$ (E = S, Se) where the cleavage products were contaminated with unidentifiable $SiMe_3$-containing species. However for these compounds the formed binary chalcogenides SnE (E = S, Se) also proved to be extremely rich in elemental tin which was in our case only observed for the vacuum thermolysis of **1**.[12]

Conclusions

Reaction of $SnCl_2$ with two equivalents of $PhESiMe_3$ (E = S, Se, Te) yielded the 1-D-tin(II) phenylchalcogenolato complexes $^1_\infty$[Sn(EPh)$_2$] in high yields. The closely related 1D chain structure of the selenolato and tellurolato complex in the solid state differ from the thiolato analogue with respect to the coordination modes of the tin atoms which is found to be larger in the case of the heavier chalcogen elements. DFT calculations reveal that the structures should be described as consisting of monomeric "$Sn(EPh)_2$" units which are linked by additional weaker chalcogen to tin donor acceptor bonds to form polymeric chains. With respect to the optical and thermal behaviour $^1_\infty$[Sn(TePh)$_2$] shows a significant red shift of the absorption onset and a distinctly reduced thermal stability compared to the other two homologues. While thermal treatment of the tellurolate complex

leads under comparable mild conditions (200 °C, N_2) to the almost stoichiometric formation of SnTe and $TePh_2$ the other reactions are ongoing from the tellurolato to the thiolato complex and by the use of vacuum conditions increasingly dominated by sublimation. In addition investigations of the volatile reaction products suggest more complex reactions in the gas phase than the formal stoichiometric cleavage of EPh_2 (E = S, Se, Te) with formation of SnE. However the investigations suggest that more easily sublimable compounds $[Sn(ER)_2]$ (E = S, Se; R = alkyl group) could have a potential for the use as single source precursor compounds for the synthesis of SnE in CVD processes.

Experimental Section

Synthesis: Standard Schlenk techniques were employed throughout the syntheses using a double manifold vacuum line (10^{-3} mbar) with high purity nitrogen (99.99990%). The solvents thf (tetrahydofuran), dme (1,2-dimethoxyethan) and ethyl ether were dried with sodium-benzophenone, and distilled under nitrogen. $PhSSiMe_3$ and $SnCl_2$ were purchased from Aldrich. $PhSeSiMe_3$[44] and $PhTeSiMe_3$[45] were prepared according to literature procedures.

[Sn(SPh)$_2$] (1): $SnCl_2$ [0.162 g (0.85 mmol)] is dissolved in 10 mL of dme to give a clear solution. Upon addition of $PhSSiMe_3$ [0.34 mL (1.79 mmol)] tiny yellow needles soon start to crystallize from the solution. Filtration and washing with ethyl ether after two days resulted in 0.20 g of **1**. Evaporation of the pure filtrate to dryness, redissolution of the solid residue in 10mL of thf and layering with ethyl ether yielded further 0.03g of **1** to give a total yield of 81%. **1** is soluble in thf, slightly soluble in dme and not soluble in ethyl ether. $C_{12}H_{10}S_2Sn$ (337.01): calcd. C 42.8, H 3.0, S 19.0; found C 42.8, H 3.0, S 19.5. M.p. 198 °C. IR (KBr): $\tilde{\nu}$ = 3053 (m, sh), 3049 (m), 3010 (w), 1938 (w, br), 1859 (w, br), 1796 (w, br), 1732 (w, br), 1572 (m), 1472 (m), 1460 (m, sh), 1433 (s), 1384 (s), 1328 (w), 1298 (m), 1263 (m), 1181 (w), 1158 (w, br), 1081 (m), 1066 (m), 1021 (m), 895 (w), 835 (w), 732 (vs), 687 (vs), 475 (s) cm^{-1}. UV/Vis (thf) $\lambda_{max} = 257$ nm; $\varepsilon = 3.4 \times 10^4$ l mol^{-1} cm^{-1}. ^{1}H NMR [300 MHz, $(CD_3)_2$SO]: δ = 7.29 (t, 1 H, *para*-C*H*), 7.38 (t, 2 H, *meta*-C*H*) , 7.52 (d, 2 H, *ortho*-C*H*) ppm. $^{13}C\{^1H\}$ NMR [75 MHz, $(CD_3)_2$SO]: δ = 127.6 (s, *para*-*C*H), 128.0 (s, *ortho*-*C*H), 129.9 (s, *meta*-*C*H), 136.2 (s, *C*SSn) ppm. ESI-TOF-MS: m/z_{exp} 109.01, rel. int. 100, (m/z_{calc} 109.01 $SC_6H_5^-$); m/z_{exp} 446.94, rel. int. 100 [m/z_{calc} 446.94 $Sn(SC_6H_5)^{3-}$].

[Sn(SePh)$_2$] (2): $SnCl_2$ [0.154 g (0.81 mmol)] is dissolved in 25 mL of thf to give a clear solution. Upon addition of $PhSeSiMe_3$ [0.34 mL (1.79 mmol)] the mixture immediately turns yellow and a voluminous precipitate forms. Standing overnight yields thin yellow needles of **2** which are filtered and washed with dme to give a total yield of 86% (0.30 g). **2** is sparingly soluble in thf and well soluble in dmf and dmso. $C_{12}H_{10}Se_2Sn$ (430.81): calcd. C 33.5, H 2.3; found C 34.2, H 2.6. IR (KBr): $\tilde{\nu}$ = 3052 (m), 3015 (w), 2980 (w), 1936 (w, br), 1865 (w, br), 1793 (w, br), 1732 (vw, br), 1631 (w), 1570 (s), 1470 (s), 1432 (m), 1384 (s), 1323 (m), 1296 (m), 1264 (w), 1178 (w), 1158 (w, br), 1097 (vw, br), 1066 (m), 1017 (m), 997 (w), 894 (w), 840 (w), 726 (vs), 686 (vs), 666 (s), 460 (s) cm^{-1}. UV/Vis (thf) λ_{max} = 266 nm; $\varepsilon = 3.6 \times 10^4$ l mol^{-1} cm^{-1}. ^{1}H NMR [300 MHz, $(CD_3)_2$SO]: δ = 7.32 (m, 3 H, *meta*-C*H*, *para*-C*H*), 7.62 (d, 2 H, *ortho*-C*H*) ppm. $^{13}C\{^1H\}$ NMR [75 MHz, $(CD_3)_2$SO]: δ = 128.3 (s, *para*-*C*H), 130 (s, *meta*-*C*H), 130.5 (s, *C*SeSn), 131.3 (s, *ortho*-*C*H) ppm. ESI-TOF-MS: m/z_{exp} 156.96, rel. int. 100, (m/z_{calc} 156.96 $SeC_6H_5^-$); m/z_{exp} 586.78, rel. int. 100 [m/z_{calc} 586.77 $Sn(SeC_6H_5)^{3-}$].

[Sn(TePh)$_2$] (3): To a solution of $SnCl_2$ [0.38 g (1.983 mmol)] in 160 mL of thf $PhTeSiMe_3$ [0.96 mL (4.17 mmol)] is added at –70 °C. Soon the reaction solution turns orange and a voluminous precipitate forms. The reaction solution is warmed up to 4 °C overnight without stirring and then kept at this temperature in a refrigerator. Tiny yellow needles of **3** form in a deep dark yellow solution which are filtered cool and quickly washed with a 1:1 mixture of thf/dme (cooled to –5 °C) to give a total yield of 82% (0.862 g). **3** is slightly soluble in thf and well soluble in dmso. However all solutions show upon standing decomposition with formation of SnTe. $C_{12}H_{10}SnTe_2$ (528.09): calcd. C 27.3, H 1.9; found C 27.2, H 2.0. IR (KBr): $\tilde{\nu}$ = 3035 (m), 3025 (w), 2973 (w), 1940 (w, br), 1865 (w, br), 1800 (vw, br), 1566 (s), 1498 (vw), 1467 (s), 1428 (m), 1384 (s), 1322 (m), 1294 (m), 1262 (w), 1173 (w), 1157 (w), 1059 (vw, br), 1013 (m), 996 (w), 900 (w), 836 (w), 802 (w), 727 (vs), 689 (vs), 649 (m), 450 (s) cm^{-1}. UV/Vis (thf) λ_{max} = 402 nm (br); $\varepsilon = 0.0988 \times 10^4$ l mol^{-1} cm^{-1}, λ = 278 nm (sh); $\varepsilon = 0.7888 \times 10^4$ l mol^{-1} cm^{-1}, λ_{max} = 233 nm (sh); $\varepsilon = 1.172 \times 10^4$ l mol^{-1} cm^{-1}. ^{1}H NMR [300 MHz, $(CD_3)_2$SO]: δ = 7.0 (t, 2 H, *meta*-C*H*), 7.11 (1 H, *para*-C*H*), 7.68 (d, 2 H, *ortho*-C*H*) ppm. $^{13}C\{^1H\}$ NMR [75 MHz, $(CD_3)_2$SO]: δ = 114 (s, *C*TeSn), 125.7 (s, *para*-*C*H), 129 (s, *meta*-*C*H), 139.3 (s, *ortho*-*C*H) ppm. ESI-TOF-MS: m/z_{exp} 206.95, rel. int. 100, (m/z_{calc} 206.95 $TeC_6H_5^-$); m/z_{exp} 324.85, rel. int. 25, (m/z_{calc} 324.85 $TeSnC_6H_5^-$); m/z_{exp} 734.74, rel. int. 50 [m/z_{calc} 734.74 $Sn(TeC_6H_5)^{3-}$].

Thermolysis: Thermolysis experiments were carried out using a Linn High Term FRHT-70/500/1100 programmable tube furnace, 70 cm long and 4 cm in diameter equipped with a ca. 50 × 3 cm borosilicate Schlenk tube. For experiments under vacuum the tube was directly connected with a cool trap to a turbo molecular pump setup from Edwards (vacuum 10^{-6} mbar) while for thermolysis under nitrogen the tube with the cool trap were connected via a Viton tubing to a mercury bubbler of a Schlenk line. The samples to be pyrolysed were placed in either quartz or porcelain boats in the center of the furnace (ca. 200 mg). For all samples the oven was programmed to ramp at a rate of 2 °C/min to 350 °C under a static pressure of N_2 and to 300 °C under vacuum (2×10^{-6} mbar) and hold at this temperature for 1h before allowing the oven to cool to room temperature. The solid residues in the porcelain or quartz boats were weighed and characterized by powder X-ray analyses while the volatile cleavage products which deposit in the part of the tube outside the furnace and in the cool trap were collected with thf (liquid products) for NMR and ESI-TOF analysis or investigated by powder XRD in the case of solids.

Details of the Thermolysis of 1: The cleavage products of **1** could by careful condensation be almost completely separated in a yellow powder and a pale yellow liquid. The liquid contains beside the main product SPh_2[46,47] other products with aromatic C and H atoms which could not be identified by NMR spectroscopy. The XRD powder pattern of the yellow powder reveals the existence of crystalline material however it does not match that of **1**. ESI-TOF mass spectra of solutions of this powder in thf show SPh^- ions (m/z_{calc} 109.01, m/z_{exp} 108.99, rel. int. 44) but do not display the characteristic fragment $[Sn(SPh)_3]^-$ (m/z_{calc} 446.94, m/z_{exp} 446.94) which was found as the major component beside SPh^- in solutions of 1. Instead other fragments which contain tin atoms and a higher S:C/H ratio were found like $SnS_3C_6H_7^-$ (m/z_{calc} 294.87, m/z_{exp} 294.84 rel. int. 11), $SnS_3C_{12}H_9^-$ (m/z_{calc} 368.89, m/z_{exp} 368.88 rel. int. 100), $SnS_5C_{18}H_{13}$ (m/z_{calc} 508.86, m/z_{exp} 508.86 rel. int. 40) and $SnS_6C_{24}H_{17}$ (m/z_{calc} 616.87, m/z_{exp} 616.86 rel. int. 4). Suggestions

for the structures of these fragments are difficult to make because no other S, C, H containing ligands could be identified in the mass spectra.

Crystallography: Crystals suitable for single-crystal X-ray diffraction were taken directly from the reaction solution of the compound and then selected in perfluoroalkylether oil. Single-crystal X-ray diffraction data of **1** and **2** were collected using graphite-monochromatised Mo-K_α radiation (λ = 0.71073 Å) on a STOE IPDS II (Imaging Plate Diffraction System). Single-crystal X-ray diffraction data of **3** were collected using synchrotron radiation (λ = 0.80 Å) on a STOE IPDS II (Imaging Plate Diffraction System) at the ANKA synchrotron source in Karlsruhe. Raw intensity data were collected and treated with the STOE X-Area software Version 1.39. Data for all compounds were corrected for Lorentz and polarisation effects. Based on a crystal description numerical absorption corrections were applied for **1** and **3** (Table 3).[48] The structures were solved with the direct methods program SHELXS of the SHELXTL PC suite programs,[49] and were refined with the use of the full-matrix least-squares program SHELXL. Molecular diagrams were prepared using Diamond.[50]

Table 3. Crystallographic data for $^1_\infty$[Sn(SPh)$_2$] (**1**), $^1_\infty$[Sn(SePh)$_2$] (**2**) and $^1_\infty$[Sn(TePh)$_2$] (**3**).

	1	**2**	**3**
fw [g/mol]	337.01	430.81	528.09
Crystal system	orthorhombic	monoclinic	monoclinic
Space group	$Pca2_1$	$P2_1/n$	$P2_1/n$
Cell			
a [Å]	7.141(1)	11.708(2)	12.389(3)
b [Å]	6.110(1)	11.893(2)	11.833(2)
c [Å]	26.740(5)	18.427(4)	18.504(4)
β [°]		93.32(3)	101.89(3)
V [Å^3]	1166.8(4)	2561.3(9)	2654.5(9)
Z	4	8	8
T [K]	190	150	130
λ [Å]	MoK_α	MoK_α	0.8000
d_c [g cm^{-3}]	1.919	2.234	2.643
$\mu(\lambda)$ [mm]$^{-1}$	2.509	7.644	8.651
F(000)	656	1600	1888
$2\theta_{max}$ [°]	49	52	56
Measured reflns.	3512	17192	12661
Unique reflns.	1851	4805	4379
R_{int}	0.0516	0.0350	0.0535
Reflns. with $I > 2\sigma(I)$	1755	4172	3930
Refined params.	137	351	351
$R1[I > 2\sigma(I)]$[a]	0.0373	0.0242	0.0272
$wR2$(all data)[b]	0.0996	0.0565	0.0688
Abs. struct. param.	0.55		

[a] $R_1 = \Sigma||F_o| - |F_c||/\Sigma|F_o|$. [b] $wR_2 = \{\Sigma[w(F_o^2 - F_c^2)^2]/\Sigma[w(F_o^2)^2]\}^{1/2}$.

All Sn, S, Se, Te, and C atoms were refined with anisotropic displacement parameters whilst H atoms were located in the difference fourier map and freely refined for **2** and **3** and calculated in fixed positions for **1**.

CCDC-724254(**1**), –724255(**2**) and –724256(**3**) contain the supplementary crystallographic data for this paper. These data can be obtained free of charge from The Cambridge Crystallographic Data Centre via www.ccdc.cam.ac.uk/data_request/cif.

X-ray powder diffraction patterns (XRD) for $^1_\infty$[Sn(SPh)$_2$] (**1**), $^1_\infty$[Sn(SePh)$_2$] (**2**) and $^1_\infty$[Sn(TePh)$_2$] (**3**) were measured on a STOE STADI P diffractometer (Cu-$K_{\alpha1}$ radiation, Germanium monochromator, Debye–Scherrer geometry) in sealed glass capillaries which agree with the theoretical powder diffraction patterns which were calculated on the basis of the atom coordinates obtained from single-crystal X-ray analysis by using the program package STOE WinXPOW.[51]

Physical Measurements: C, H, S elemental analyses were performed on an "Elementar vario Micro cube" instrument.

UV/Vis absorption spectra of **1**–**3** in solution were measured on a Varian Cary 500 spectrophotometer in quartz cuvettes. Solid state absorption spectra were measured as micron sized crystalline powders between quartz plates with a Labsphere integrating sphere.

^{1}H-NMR and ^{13}C-NMR spectra were recorded on a Bruker DPX Avance 300.

IR spectra were measured on a Perkin–Elmer Spectrum GX as KBr pellets in a region from 4000 to 350 cm^{-1}.

Thermogravimetric analyses were run in Al_2O_3 crucibles on a thermobalance STA 409 from Netzsch in vacuo (7×10^{-6} mbar) or with a dynamic helium gas flow (25 mL/ min) at a heating rate of 2 °C/min. The crucibles were filled (20–35 mg) inside an argon glove box, transferred in Schlenk tubes and mounted under a stream of argon to the balance. However trace contamination of oxygen indicated by the formation of SnO and SnO_2 could not be totally avoided in this way in all cases. Caution should be taken with respect to the toxic and bad smelling volatile products formed in the thermolysis.

Mass spectra were taken on a Time of Flight (TOF) mass spectrometer (Bruker Daltonics, MicroTOF-QII) equipped with an electrospray ion source (off axis sprayer). The solutions were sprayed at typical flow rates of about 180 μL/h and nebulized using dry nitrogen. The desolvation glass capillary was heated to 180 °C. For all ion signals observed the charge state was immediately evident from their isotopomere splitting and assignment to an ionic species was unequivocally confirmed by comparison to the computed isotopic distribution. All *m*/*z* values given in the text correspond to the most abundant peak of the respective distributions.

Acknowledgments

This work was supported by the National Science Foundation of China (Grant 20525310, 20773167) the Deutsche Forschungsgemeinschaft (center for functional nanostructures CFN) and the Research Center of Karlsruhe. The authors are grateful to E. Tröster and N. Metz for their valuable assistance in the practical work.

[1] I. Dance, K. Fisher, *Prog. Inorg. Chem.* **1994**, *41*, 637–803.
[2] S. Dehnen, A. Eichhöfer, D. Fenske, *Eur. J. Inorg. Chem.* **2002**, 279–317.
[3] M. W. DeGroot, J. F. Corrigan, *Comprehensive Coordination Chemistry II*; M. Fujita, A. Powell, C. Creutz (Eds.); Pergamon: Oxford, U. K., **2004**; Vol. 7, pp. 57–123.
[4] J. Arnold, *Prog. Inorg. Chem.* **1995**, *43*, 353–417.
[5] M. Bochmann, *Chem. Vap. Deposition* **1996**, *2*, 85–96.
[6] B. Krebs, G. Henkel, *Angew. Chem.* **1991**, *103*, 785–804; *Angew. Chem. Int. Ed. Engl.* **1991**, *30*, 769–788.
[7] B. Krebs, G. Henkel, *Chem. Rev.* **2004**, *104*, 801–824.
[8] G. Barone, T. G. Hibbert, M. F. Mahon, K. C. Molloy, L. S. Price, I. P. Parkin, A. M. E. Hardy, M. N. Field, *J. Mater. Chem.* **2001**, *11*, 464–468.
[9] D. H. R. Barton, H. Dadoun, *New J. Chem.* **1982**, *6*, 53–57.
[10] S. Schlecht, M. Budde, L. Kienle, *Inorg. Chem.* **2002**, *41*, 6001–6005.
[11] Y. Cheng, T. J. Emge, J. G. Brennan, *Inorg. Chem.* **1996**, *35*, 342–346.
[12] A. L. Seligson, J. Arnold, *J. Am. Chem. Soc.* **1993**, *115*, 8214–8220.

[13] D. E. Fenton, R. R. Gould, P. G. Harrison, T. B. Harvey, G. M. Omletanski, K. C.-T. Sze, J. J. Zuckerman, *Inorg. Chim. Acta* **1970**, *4*, 235–243.
[14] P. G. Harrison, S. R. Stobart, *Inorg. Chim. Acta* **1973**, *7*, 306–310.
[15] M. E. Peach, *J. Inorg. Nucl. Chem.* **1979**, *41*, 1390–1392.
[16] J. L. Hencher, M. Khan, F. F. Said, R. Sieler, D. G. Tuck, *Inorg. Chem.* **1982**, *21*, 2787–2791.
[17] J. J. Arsenault, P. A. W. Dean, *Can. J. Chem.* **1983**, *61*, 1516–1523.
[18] P. B. Hitchcock, M. F. Lappert, B. J. Samways, E. L. Weinberg, *J. Chem. Soc., Chem. Commun.* **1983**, 1492–1494.
[19] M. Veith, P. Hobein, R. Rösler, *Z. Naturforsch., Teil B* **1989**, *44*, 1067–1081.
[20] N. N. Zemlyanskii, I. V. Borisova, M. G. Kuznetsova, E. N. Khrustalev, M. Yu. Antipin, Yu. A. Ustynyuk, E. E. Lunin, C. Eaborn, M. S. Hill, J. D. Smith, *Russ. J. Org. Chem.* **2003**, *39*, 491–500.
[21] P. A. W. Dean, J. J. Vittal, N. C. Payne, *Can. J. Chem.* **1985**, *63*, 394–400.
[22] J. Lee, T. J. Emge, J. Brennan, *Inorg. Chem.* **1997**, *36*, 5064–5068.
[23] TURBOMOLE V6.0, TURBOMOLE GmbH Karlsruhe, **2009**, http://www.turbomole.de. TURBOMOLE is a development of University of Karlsruhe and Forschungszentrum Karlsruhe, **1989–2007**, TURBOMOLE GmbH since **2007**.
[24] A. D. Becke, *J. Chem. Phys.* **1993**, *98*, 5648–5652.
[25] J. P. Perdew, *Phys. Rev. B* **1986**, *33*, 8822–8824.
[26] F. Weigend, R. Ahlrichs, *Phys. Chem. Chem. Phys.* **2005**, *7*, 3297–3305.
[27] F. Weigend, *Phys. Chem. Chem. Phys.* **2006**, *8*, 1057–1065.
[28] B. Metz, H. Stoll, M. Dolg, *J. Chem. Phys.* **2000**, *113*, 2563–2569.
[29] K. A. Peterson, D. Figgen, E. Goll, H. Stoll, M. Dolg, *J. Chem. Phys.* **2003**, *119*, 11113–11123.
[30] J. Pipek, P. G. Mezey, *J. Chem. Phys.* **1989**, *90*, 4916–4926.
[31] R. Mulliken, *J. Chem. Phys.* **1955**, *23*, 1833–1840.
[32] J. P. Foster, F. Weinhold, *J. Am. Chem. Soc.* **1980**, *102*, 7211–7218.
[33] P. S. DelBucchia, J. C. Jumas, M. Maurin, *Acta Crystallogr., Sect. B* **1981**, *37*, 1903–1905.
[34] K. Adouby, C. Perez-Vicente, J. C. Jumas, *Z. Kristallogr.* **1998**, *213*, 343–349.
[35] T. S. Yeoh, S. G. Teoh, H. K. Fun, *J. Phys. Soc. Jpn.* **1988**, *57*, 3820–3823.
[36] M. Scheer, G. McCarthy, D. Seidler, P. Boudjouk, *Chem. Mater.* **1994**, *6*,2108–2112.
[37] S. Perumal, R. Chandrasekaran, V. Vijayabaskar, D. A. Wilson, *Magn. Reson. Chem.* **1995**, *33*, 779–790.
[38] S.-K. Chung, K. Sasamoto, *J. Org. Chem.* **1981**, *46*, 4590–4592.
[39] H. E. Swanson, E. Tatge, Natl. Bur. Stand. (U. S.), Circ. 539, I (**1953**), 24–27.
[40] M. R. Dettig, M. D. Seidler, *J. Org. Chem.* **1982**, *47*, 1354–1356.
[41] D. J. Gulliver, E. G. Hope, W. Levason, *J. Chem. Soc., Perkin Trans. 2* **1984**, *3*, 429–434.
[42] Th. Arnauld, D. H. R. Barton, J. F. Normant, *J. Org. Chem.* **1999**, *64*, 3722–3725.
[43] R. K. Chadha, J. M. Miller, *J. Chem. Soc., Dalton Trans.* **1982**, 117–120.
[44] N. Miyoshi, H. Ishii, K. Kondo, S. Mui, N. Sonoda, *Synthesis* **1979**, 301–304.
[45] J. E. Drake, R. T. Hemmings, *Inorg. Chem.* **1980**, *19*, 1879–1883.
[46] S. Perumal, R. Chandrasekaran, V. Vijayabaskar, D. A. Wilson, *Magn. Reson. Chem.* **1995**, *33*, 779–790.
[47] S.-K. Chung, K. Sasamoto, *J. Org. Chem.* **1981**, *46*, 4590–4592.
[48] *X-RED32 1.01*, Data Reduction Program, Stoe & Cie GmbH, Darmstadt, Germany, **2001**.
[49] G. M. Sheldrick, *SHELXTL PC version 5.1*, An Integrated System for Solving, Refining, and Displaying Crystal Structures from Diffraction Data, Bruker Analytical X-ray Systems, Karlsruhe, **2000**.
[50] *Diamond Version 2.1d*, K. Brandenburg, Crystal Impact GbR, **1996–2000**.
[51] *STOE*, *WinXPOW*, STOE & Cie GmbH, Darmstadt, **2000**.

Received: September 21, 2009
Published Online: December 10, 2009

